Energy & Environmental Science

Supporting Information

Modelling the morphology and thermomechanical behaviour of low-bandgap conjugated polymers and bulk heterojunction films

Samuel E. Root,[a] Nicholas Jackson,[b] Suchol Savagatrup,[a] Gaurav Arya,[a]* and Darren J. Lipomi[a]*

---

1. Simulation Details

1.1 General Remarks. In all the simulations described in this article the following algorithms and software were used.

1) The shake algorithm was employed to constrain bonds containing Hydrogen atoms to fixed distances. The algorithm used is standard in the LAMMPS simulation package.

2) The Velocity Verlet algorithm was used for integrating the equations of motion

3) The Particle-Particle/Particle-Mesh (PPPM) algorithm was used for treating long-range electrostatic interactions.

4) The molecular dynamics simulation package LAMMPS was used for all simulations.[1]

5) The visualization package OVITO was used for all visualizations.[2]

6) Simulation initialization and post-processing was performed using custom python scripts.

7) All uncertainty quantification was performed by taking the average and standard deviation from a total of three randomly generated initial configurations subjected to analogous MD simulation protocols.

1.2 Melt Phase System Initialization. Isolated chains in the fully extended conformation were first subjected to elevated temperature (800 K) simulations using Langevin dynamics (damping parameter = 3800 fs, time step = 2 fs). Random conformations were outputted on nanosecond intervals. This protocol resulted in 60 uncorrelated chain conformation for each polymer simulated. These chains were next assigned a randomly generated centre of mass and orientation with respect to an orthorhombic, periodic simulation box at a mass density of 0.01 g cm^{-3}. Placement of chains was constrained such that no two atoms on different chains were within 20 Å of another. This was especially important for simulations containing $PC_{71}BM$, as to avoid spearing the fullerene cage, which would result in unstable dynamics. The randomly generated configurations were next subjected to a conjugate-gradient energy minimization to further ensure that there were no unphysical interactions to make the simulation unstable in the first couple of time steps. Next, the temperature was ramped from 0 to 800 K over the course of 1 ns using Langevin dynamics (damping parameter = 3800 fs, dielectric constant = 9.8). Next, a Nosé-Hoover style barostat (time constant = 1000 fs) was used to relax the simulation box at 1 atmosphere of pressure until the density converged to the equilibrium melt-phase value at 800 K and 1 atm over the course of 5 ns. For all bulk heterojunction simulations, a mass fraction of 1:1.5 polymer: PCBM was used. This composition is consistent with experimentally optimized devices.

1.3 Equilibrium Sampling Parameters. A Nosé-Hoover style thermostat (time constant = 100.0 fs) and barostat (time constant = 1000.0 fs) was used to simulate the NPT equilibrium dynamics of the polymeric melts and composites. The dielectric was set to 1.0 and a Verlet neighbour list was employed for MPI parallelization. Simulations were run using 24 processors. A time step of 1.5 fs was used for the remaining simulations.

1.4 Annealing Protocol. The melt-phase structures were subjected to an annealing protocol in which the temperature was ramped in 20 K intervals from 800 K to 100K using 1 ns for both the ramping and equilibration runs. All of the thermodynamic parameters were outputted periodically (0.01 ns intervals). This resulted in a total of 70 ns of simulation for each system. The configurations obtained at 600 K were further subjected to 5 ns of dynamics to generate the equilibrium melt-phase statistics presented in the main document. The configurations obtained at 300 K (in the glassy state) are denoted as the *melt-quenched* morphology (**Figure S1**) and were used for the uniaxial tensile loading simulations.

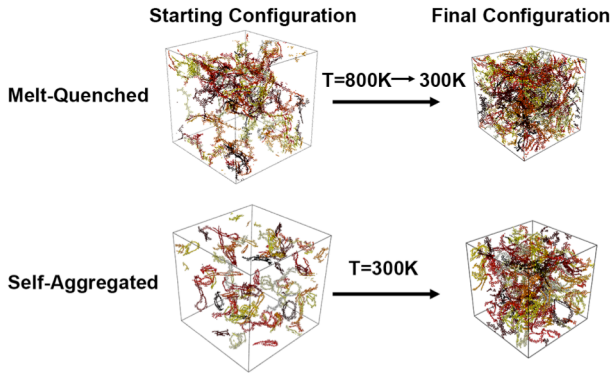

Figure S1. Trajectory snapshots illustrating the difference between the two simulation protocols employed in this work. While neither morphology is in a state of equilibrium, the *self-aggregated* morphology is further from equilibrium than the *melt-quenched* morphology.

1.5 Determination of Glass Transition Temperature. The glass transition temperature for each system was computed by taking the average density from the second half (0.5 ns) of the annealing simulations and plotting the results against the temperature. A custom algorithm was used to perform a bilinear regression on the data and find the best fit to both the melt and glassy regions. The glass transition temperature was taken as the intersection of the linear fits. The algorithm works by scanning through all the possible bilinear regressions and finding the one that gave the maximum value for the sum of the R^2 values as shown in **Figure S2a**. A spacing of 16 data points between linear fits was used due to the width of the glass transition region that results from the rapid quenching (**Figure S2b)**.

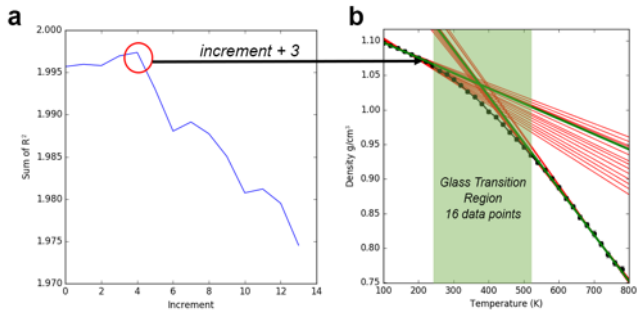

Figure S2. Schematic diagram illustrating algorithm for predicting the glass transition temperature from simulation data (TQ1). (a) Plot of sum of R^2 of the two fits against the increment of fitting. (b) Corresponding thermal data showing non-optimal fits in red and optimal fit in green.

1.6 Isolated Chain Simulated Annealing. Simulated annealing was performed on individual chains in the implicitly solvated state. A dielectric constant of 4.8 and a damping parameter of 3800 fs was used with Langevin dynamics to mimic the effect of dissolution in chloroform. The same chains conformations generated from the melt-phase initialization were subjected to further randomization at 800 K for 1 ns and then linearly cooled to 300 K over the course of 5 ns to generate folded configurations. Simulations were repeated 60 times per polymer chain.

1.7 Self-Aggregated Morphology Initialization. The *self-aggregated* morphology was initialized using the 60 independently generated chain conformations, outputted in the isolated chain annealing simulations described in the previous section. These chain conformations were also used to gather the statistics for the conformational class analysis shown in **Figure 7a** of the main text. The chain conformations were randomly oriented and positioned in an orthorhombic, periodic simulation box subject to a non-overlapping condition at a mass density of 0.01g cm^{-1}. NPT dynamics were run using a Nosé-Hoover style thermostat (time constant = 100.0 fs) and barostat (time constant = 1000.0 fs) until the density converged (5 ns). The morphologies generated contained large voids, and were far from equilibrium. A schematic representation of the simulation protocol is given in **Figure S1.**

Uniaxial Tensile Loading. The mechanical deformation simulations were run by imposing a constant strain rate ($1x10^{-6}$ Å ps^{-1}) in the x-dimension and applying a stress-free boundary condition in both transverse dimensions. The stress-strain curve was obtained using a moving average (window size = 1000 fs, 10 fs increments) of axial component of the virial stress tensor, as described previously.[3]

2. In-Depth Analysis of Simulation Results

2.1 Dihedral Statistics. The dihedral probability distributions obtained from the melt-phase simulations (T=600 K, p=1 atm) can be further analysed to obtain the fraction of conjugated unit pairs in syn vs. anti and conjugated vs. non-conjugated conformations. The results of our analysis are shown in **Table 1**. Based on this data we see that TQ1 has the highest preference of Syn conformations, while PTB7 and PDTSTPD have similar conformational preferences. Additionally, we see that PDTSTPD is the most conjugated followed by PTB7 and TQ1. These conformational statistics represent testable predictions by means of NMR spectroscopy as described by Do and co-workers.[4]

Table S1. Quantitative analysis of dihedral statistics obtained at (T = 600K, p= 1 atm).

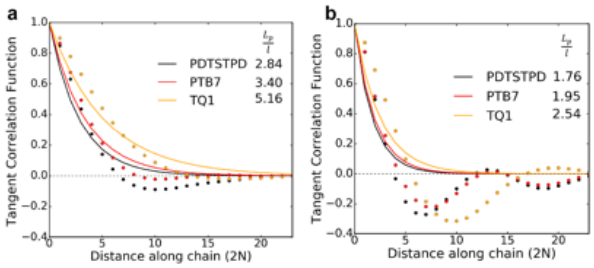

Table S2. Coefficients obtained from fitting tangent correlation functions to equation (3).

	Polymer	l (Å)	A_1	L_{p1}/l	λ_{p1}/l	A_2	L_{p2}/l	λ_{p2}/l	A_3	L_{p3}/l	λ_{p3}/l	Sum of R^2
Kinetic	PDTSTPD	6.01	0.80	7.04	2.22	0.16	29.55	4.8	0.04	7.17	1.10	0.0003
	PTB7	6.4	0.51	9.07	2.22	0.39	10.45	4.54	0.10	4.54	1.07	0.0004
	TQ1	4.2	0.55	11.25	4.54	0.43	12.43	2.85	0.02	3.43	1.30	6e-05
Thermodynamic	PDTSTPD	6.01	.82	5.77	4.87	0.19	5.9	2.48	0.0	-	-	0.0008
	PTB7	6.4	0.56	5.65	3.22	0.45	8.16	9.98	0.0	-	-	0.0009
	TQ1	4.2	0.63	7.86	5.05	0.377	16.2	14.51	0.0	-	-	7.9e-05

Polymer	Syn	Anti	Non	Conj
PTB7 (AD)	0.25	0.39	0.36	0.64
PTB7 (DA)	0.40	0.37	0.22	0.77
PTB7 (AVG)	0.325	0.38	0.29	0.7
TQ1	0.50	0.18	0.32	0.68
PDTSTPD	0.37	0.35	0.277	0.72

Figure S3. Plots showing fits tangent correlation functions obtained from the (a) melt-phase and the (b) isolated chain annealing simulations to an exponentially decaying function. It can be clearly seen that the worm-like chain model cannot be used to adequately describe these chains.

2.2 Tangent Correlation Function Fitting. One of the most interesting findings that resulted from our simulations was the observation of oscillatory tangent correlation functions in the melt and isolated chain states. For typical semi-flexible polymers, the tangent correlation function can be fit to an exponential decay to find the persistence length. As shown in **Figure 3**, an exponential decay did not give a satisfactory fit to the simulation data. The tangent correlation function of a worm-like chain can be expressed as:

$$\langle \hat{\mathbf{t}}_\mathbf{i} \cdot \hat{\mathbf{t}}_\mathbf{i+j} \rangle_j = e^{-\frac{lj}{L_p}} \qquad (1)$$

where $\hat{t}_i$ is the unit tangent vector of ith unit, L_p is the persistence length, and l is the monomer length which we took to be the average of the length of the donor and the acceptor.

A literature search subsequently revealed that an oscillatory tangent correlation function has been derived analytically for a ribbon-like chain.[5] This behaviour is apparently the result of a coupling between torsional and bending degrees of freedom. An analytical solution for the tangent correlation function of a "developable ribbon" is given by the following functional form:

$$\langle \hat{\mathbf{t}}_\mathbf{i} \cdot \hat{\mathbf{t}}_\mathbf{i+j} \rangle_j = e^{-\frac{lj}{L_p}} \cos\left(\frac{lj}{\lambda}\right) \qquad (2)$$

Here ω is the folding wavelength. In the limiting case of $\frac{L_p}{\lambda} \rightarrow 0$, this equation reduces to (1). Fits of this functional form to the simulation data for both morphologies are given in **Figure 4**. They are clearly better than a worm-like chain, however, they are still not perfect. Especially for the chains in the *self-aggregated* morphology.

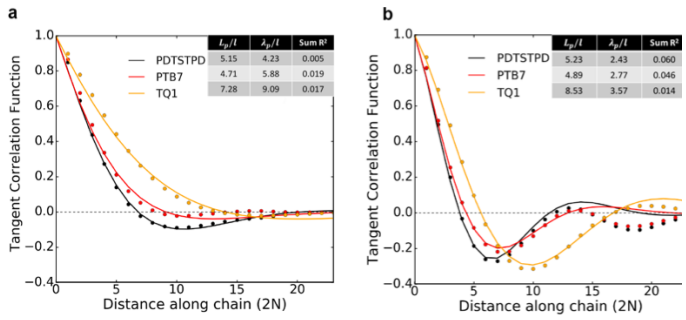

Figure S4. Plots showing fits of tangent correlation functions obtained from the (a) melt-phase and the (b) isolated chain annealing simulations to an exponentially decaying cosine function.

Even with the imperfect fit, this model enables a quantitative comparison of the stiffness and folding wavelength of these polymers. We find that in both morphologies TQ1 is the stiffest and has the longest folding wavelength. On the other hand, PDTSTPD (which is known experimentally to be the most ordered of the three) has shortest folding wavelength and shortest persistence length. PTB7 is intermediate in both cases.

The imperfect fitting of equation (2) to the simulation data implies that there are multiple modes of tangent correlation decay and folding in these polymers. We found that a series expansion of equation (2) into equation (3) gave excellent fits to the simulation data, as shown in the main text.

$$\langle \hat{\mathbf{t}}_i \cdot \hat{\mathbf{t}}_{i+j} \rangle_j = \sum_{n=1}^{3} A_n e^{-jl/L_{pn}} \cos(lj/\lambda_n) \qquad (3)$$

All fits were performed using the curve_fit() function available in the Scipy module for Python. This function performs a non-linear least squares algorithm. The quality of the fit can be determined by the sum of the residuals squared (Sum R^2). A smaller Sum R^2 signifies a better fit. As shown in **Table S2**, fits of eq (3) to the data provide the best fits, although eq (2) still provides a reasonable fit (**Figure S4**).

2.3 Ramachandran Plots. To investigate the handedness of the helical polymer structure, we borrowed a technique commonly used in the analysis of protein structures. A Ramachandran plot is a 2D correlation map of two consecutive dihedral angles along the contour of the polymer back bone.[6] The presense of asymetry in the correlation map indicates the handedness (or lack thereof) of the helical pitch. Ramachandran plots obtained from the melt phase are shown in **Figure S5.** We used a bin size of 10 degrees to compute the 2D histogram. We found that the plots exhibited symetric correlations, indicating that the helices have no preferred handedness.

2.4 Pair Distribution Functions. The pair distribution functions shown in Figure 4 of the main text were calculated by first finding the centre of mass of each donor, acceptor, and C70 fullerene unit. Next all of the pairwise distances were binned using an increment of $\boldsymbol{\delta}$ =0.5Å into a histogram of intermolecular **separations**, $\boldsymbol{C_i}$. Finally we applied equation (4) to average and normalize $\boldsymbol{C_i}$ over each simulation snapshot to calculate the pair distribution function:

$$g_{\alpha\beta}(i\delta) = \frac{C_i}{\tau N_\alpha N_\beta} \times \frac{V}{\frac{4\pi}{3}\delta^3((i+1)^3 - i^3)} \qquad (4)$$

Here N_α, N_β are the number of particles of type α, β in the system (for the case $\alpha = \beta$, $N_\beta \rightarrow (N_\alpha - 1)/2$), τ is the number of frames that were averaged over, and V is the volume of the simulation box. Pair distribution functions shown were averaged over three independent initial configurations to obtain smooth distributions. We note, however, that the features were observed to be consistent between these runs indicating that the systems were well-equilibrated in the melt phase at 600K and 1atm.

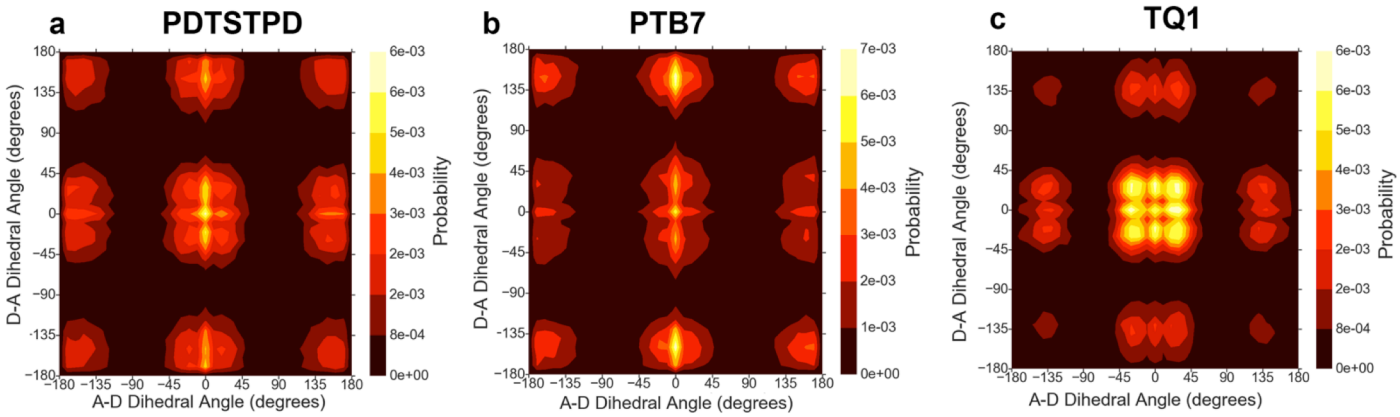

Figure S5. Ramachandran plots showing correlation maps for consecutive dihedral angles along the polymer backbones. a) PDTSTPD, b) PTB7 and c) TQ1.

For the acceptor unit of both PTB7 and PDTSTPD we observed a broad peak in the pair distribution function at a distance of 13 and 14 Å respectively. We have rationalized these peaks geometrically as evidence of inter-digitation of side chains. As can be seen in

Figure S6, when the side chains of the acceptor unit of PDTSTPD are stacked, the acceptor units are separated by ~14Å.

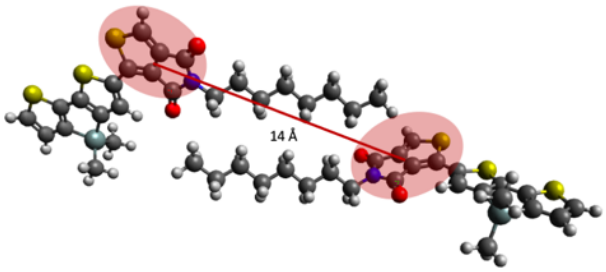

Figure S6. Diagram illustrating argument ascribing the broad peak in the pair distribution function for PDTSTPD to side chains interdigitating. A similar argument can be made for PTB7.

2. 5 Classification of Chain Conformations. The chain conformations produced from the isolated chain annealing simulations were classified as either globular, toroidal, folded, or extended according to an analysis of their size, order, and pattern of the orientational contact maps (shown in the main text). We employed the Landau-De Gennes **Q**-tensor to characterize the conformational order present in the isolated chain aggregates.[7] This generalized order parameter can be written as:

$$Q_{\alpha\beta} = \langle \frac{3}{2}\hat{\mathbf{t}}_{\mathbf{i\alpha}}\hat{\mathbf{t}}_{\mathbf{i\beta}} - \frac{1}{2}\delta_{\alpha\beta} \rangle \qquad (5)$$

Here $\hat{\mathbf{t}}_{\mathbf{i\alpha}}$ represents the tangent vector of the ith unit along the backbone of the polymer, δ is the Kronecker delta, and α, β denote Cartesian dimensions. The bracket signifies an average over all the conjugated units in the polymer backbone. To compare the degree of ordering across chains, the maximum eigenvalue of this tensor, *S,* was computed. By construction, S = 1 corresponds to a perfectly straight chain and S = 0 corresponds to a completely random globule.

The sizes of the chains were compared using two metrics. The radius of gyration, and the length of the end-to-end vector, $|\vec{R}|$. The end-to-end vector was important for distinguishing between self-aggregated and extended chains. We defined the normalized end-to-end vector as $\frac{|\vec{R}|}{l}$ in order to make systematic comparisons across the three materials. Recall that l is the length of the donor and acceptor units averaged.

Extended Chains: Chains were classified as extended if $\frac{|\vec{R}|}{l}$ was greater than 6. Extended chains could be either ordered (completely straight) or disordered. The key distinguishing factor for this class of conformations was the lack of self-aggregated π-stacking.

Globular Chains: Chains were classified as globular if $\frac{|\vec{R}|}{l}$ was less than 6 and if the maximum eigenvalue of their Q-tensor was greater than 0.20. If these two conditions were met, the contact map and the 3D structure of the chain looked disordered.

Folded Chains: Chains were classified as folded if $\frac{|\vec{R}|}{l}$ was less than 6 and if the maximum eigenvalue of their Q-tensor was less than 0.20 and if the orientational contact maps exhibited a blocky structure.

Toroidal Chains: Chains were classified as toroidal if $\frac{|\vec{R}|}{l}$ was less than 6 and if the maximum eigenvalue of their Q-tensor was greater than 0.20 and if the orientational contact maps exhibited a diagonal structure.

In all cases the chains were visually inspected to ensure correct classification. We found that the most difficult conformations to distinguish were the toroidal and the folded. Threshold values could not be set, and we had to rely on visual inspection of the orientational contact maps and the 3-dimensional structure.

2.6 Self-Aggregated Morphology Statistics. Although the *self-aggregated* morphology is far from equilibrium and not amenable to efficient sampling, the large system size simulated allows us to obtain a quantitative picture of the nanoscale morphology. The results of for the intermolecular pair distribution functions and dihedral distributions are shown in **Figure S7.** It can be seen clearly that intermolecular coupling between donor and acceptor units is severely diminished. This intuitively makes sense as the self-aggregated chains have less "free" conjugated units to form intermolecular aggregates. Comparing across the three materials, we see that TQ1 retains the most intermolecular aggregates, followed by PTB7 and then PDTSPTD. This makes sense, as TQ1 had the highest fraction of globular chains and PTB7 and TQ1 both had similar fractions of extended chains. PDTSTPD on the other hand formed almost exclusively toroidal and folded chain structures.

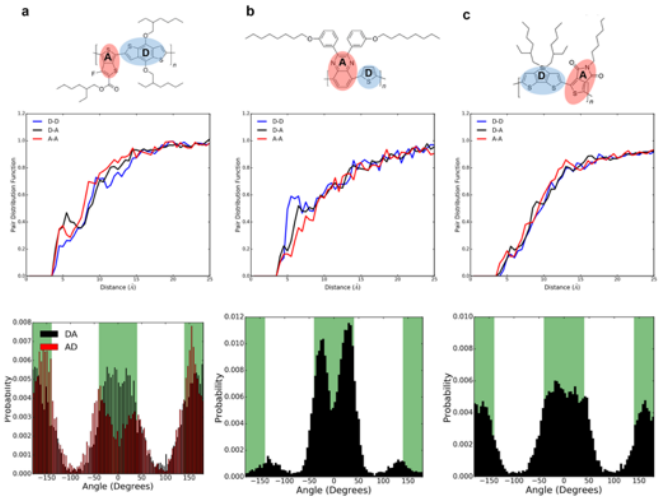

Figure S7. Results for the pair distribution functions and dihedral distributions obtained from the self-aggregated morphology of each polymer.

Additionally, there is an apparent sharpening of the dihedral distributions as the chains aggregate into minimum energy configurations without the topological constraints imposed by intermolecular interactions in the melt. It can be seen in **Table 3** that the fraction of conjugated dihedral angles is increased in the *self-aggregated* morphology when compared to the melt-phase statistics of **Table 1**. Specifically, we see that TQ1 has the largest shift towards syn conformations. This effect is further manifested in the average conjugation length of the *self-aggregated* morphology, when compared to the melt. We calculated an average conjugation length of 3.6, 3.2, and 3.4 for PDTSTPD, PTB7, and TQ1 respectively.

Table S3. Quantitative analysis of dihedral statistics obtained from the *self-aggregated* morphology (T = 300K, p= 1atm).

Polymer	Syn	Anti	Non	Conj
PTB7 (AD)	0.22	0.45	0.32	0.68
PTB7 (DA)	0.38	0.37	0.24	0.76
PTB7 (AVG)	0.3	0.41	0.28	0.72
TQ1	0.69	0.04	0.26	0.74
PDTSTPD	0.42	0.32	0.26	0.74

2.8 Bulk Heterojunction Statistics. We found that the presence of $PC_{71}BM$ served to significantly alter the structure of the polymer chains. This effect is apparent in the tangent correlation functions (**Figure S8**) obtained from the melt-phase bulk heterojunction simulations. We see both a decrease in the folding wavelength and an increase in the persistence length for all three materials when compared to the pure melt.

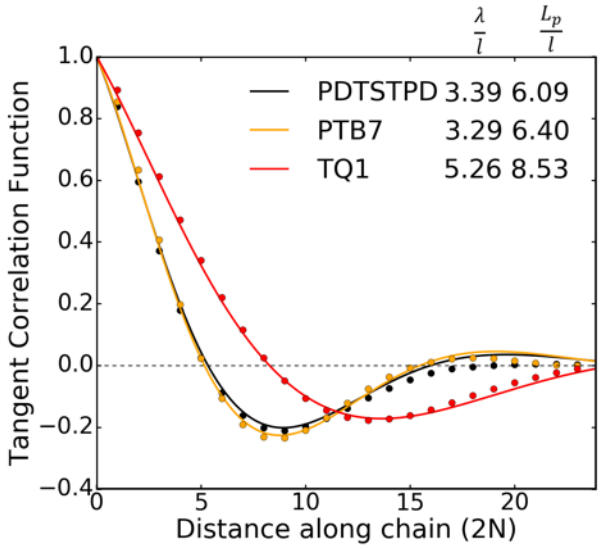

Figure S8. Tangent correlation functions obtained from melt-phase simulations of the bulk heterojunction composite. (T=600K, p = 1atm).

3. Code

The code used for running these simulations is available on the following Git repository: https://github.com/seroot/AROMODEL. This python-based software, is designed specifically to work on XSEDE supercomputing resources and is currently under active development. We encourage any researcher interested in using this software to perform similar simulations to email Samuel Root (seroot@eng.ucsd.edu) for the latest release as well as detailed instructions and eager collaboration.

4. Models

The models employed in this paper were originally developed and published by Jackson and coworkers.[8] They fall within the general classification of class2 atomistic force-fields and follow the functional form of the OPLS-AA force-field of Jorgensen and co-workers.[9] LAMMPS data files containing the topology and force-field parameters for the three polymers (12-mers) and $PC_{71}BM$ are available as Supporting Information.

5. Computational Resources

The large-scale simulations presented in this work represent a significant investment in high-performance computing resources. Single chain simulations were all run on single processors. Multi-chain simulations were all run on 24 processors using the MPI implementation of LAMMPS on the Comet supercomputer at the San Diego Supercomputer Center. The simulations proceeded at a rate 1-3 ns/day. Therefore, these simulations took >1 month to perform. In total, three polymers were simulated in three conditions, and each one was repeated three times for error quantification. This resulted in a total of 27 simulations running concurrently on 24 processors each.

References

(1) Plimpton, S. Fast Parallel Algorithms for Short-Range Molecular Dynamics. *J. Comput. Phys.* **1995**, *117*, 1–19.

(2) Stukowski, A. Visualization and Analysis of Atomistic Simulation Data with OVITO–the Open Visualization Tool. *Model. Simul. Mater. Sci. Eng.* **2010**, *18*, 1–7.

(3) Root, S. E.; Savagatrup, S.; Pais, C. J.; Arya, G.; Lipomi, D. J. Predicting the Mechanical Properties of Organic Semiconductors Using Coarse-Grained Molecular Dynamics Simulations. *Macromolecules* **2016**, *49*, 2886–2894.

(4) Do, K.; Saleem, Q.; Ravva, M. K.; Cruciani, F.; Kan, Z.; Wolf, J.; Hansen, M. R.; Beaujuge, P. M.; Brédas, J.-L. Impact of Fluorine Substituents on π-Conjugated Polymer Main-Chain Conformations, Packing, and Electronic Couplings. *Adv. Mater.* **2016**.

(5) Giomi, L.; Mahadevan, L. Statistical Mechanics of Developable Ribbons. *Phys. Rev. Lett.* **2010**, *104*, 2–5.

(6) Ramachandran, G.N. Ramakrishnan, C. Sasisekharan, V. Stereochemistry of Polypeptide Chain Konfigurations. *J. Mol. Biol.* **1963**, *7*, 95–99.
(7) Pierre-Gilles de Gennes, J. P. *The Physics of Liquid Crystals*; Clarendon, Oxford, 1974.
(8) Jackson, N. E.; Kohlstedt, K. L.; Savoie, B. M.; Olvera de la Cruz, M.; Schatz, G. C.; Chen, L. X.; Ratner, M. a. Conformational Order in Aggregates of Conjugated Polymers. *J. Am. Chem. Soc.* **2015**, *137*, 6254–6262.
(9) Jorgensen, W. L.; Maxwell, D. S.; Tirado-Rives, J. Development and Testing of the OPLS All-Atom Force Field on Conformational Energetics and Properties of Organic Liquids. *J. Am. Chem. Soc.* **1996**, *118*, 11225–11236.